Liquid Crystals

ISSN: (Print) (Online) Journal homepage: https://www.tandfonline.com/loi/tlct20

Self-assembling behaviour of new functional photosensitive cinnamoyl-based reactive mesogens

Alexej Bubnov , Martin Cigl , Nela Sedláčková , Damian Pociecha , Zuzana Böhmová & Věra Hamplová

To cite this article: Alexej Bubnov , Martin Cigl , Nela Sedláčková , Damian Pociecha , Zuzana Böhmová & Věra Hamplová (2020) Self-assembling behaviour of new functional photosensitive cinnamoyl-based reactive mesogens, Liquid Crystals, 47:14-15, 2276-2291, DOI: 10.1080/02678292.2020.1783586

To link to this article: https://doi.org/10.1080/02678292.2020.1783586

Published online: 29 Jun 2020.

LIQUID CRYSTALS
2020, VOL. 47, NOS. 14–15, 2276–2291
https://doi.org/10.1080/02678292.2020.1783586

Self-assembling behaviour of new functional photosensitive cinnamoyl-based reactive mesogens

Alexej Bubnov[a], Martin Cigl[a], Nela Sedláčková[b], Damian Pociecha[c], Zuzana Böhmová and Věra Hamplová[a]

[a]Institute of Physics of the Czech Academy of Sciences, Prague, Czech Republic; [b]Gymnázium Jiřího z Poděbrad, Studentská, Poděbrady, Czech Republic; [c]Faculty of Chemistry, University of Warsaw, Warsaw, Poland

ABSTRACT

One of the most exciting classes of organic materials that is able to self-assemble at nanoscopic scale are those exhibiting the liquid crystalline (LC) behaviour which can be distantly tuned by an external stimulus. Under UV/Vis light irradiation, the reversible photoisomerisation process can take place if the compounds possess the photosensitive group, e.g. N=N or cinnamoyl group incorporated in their molecular structure. This can drastically affect the LC behaviour. However, the compounds possessing the cinnamoyl fragment with C=C double bond are capable of both photoisomerisation and photocycloaddition processes. Several cinnamoyl-based reactive mesogens with polymerisable vinyl group have been designed; their mesomorphic and structural behaviour have been studied. Depending on the molecular structure, the reactive mesogens exhibit nematic, orthogonal smectic A and tilted smectic C phases; the kinetics of the phase transition temperatures has been checked. The structure of the mesophases is confirmed by small-angle X-ray scattering. The main objective of the present work is to contribute to better understanding of molecular structure – mesomorphic property relationship for new functional cinnamoyl-based photosensitive reactive mesogens which can be further used for design of smart self-assembling macromolecular materials.

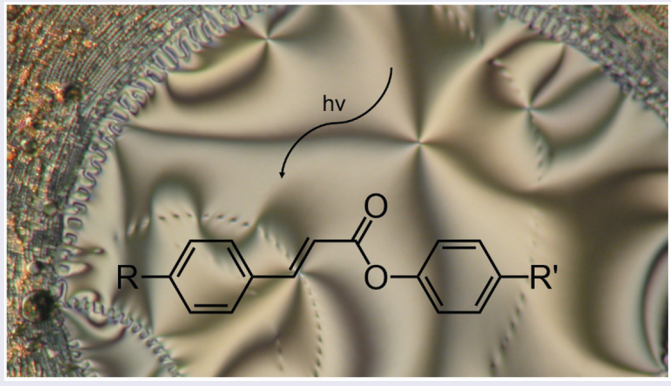

ARTICLE HISTORY
Received 28 February 2020
Accepted 13 June 2020

KEYWORDS
Liquid crystal; reactive mesogen; cinnamoyl group; photosensitive materials; self-assembling behaviour

1. Introduction

Self-organisation is a process due to which a disordered system of simple constituents can form an organised structure or pattern as a consequence of specific local interactions among those components. When the constitutive objects of such a system are molecules, the self-assembly phenomenon is a process of spontaneous, and usually reversible, organisation of molecules into ordered assemblies by non-covalent interactions. Some organic materials can exhibit the liquid crystalline (LC) behaviour, which is a specific example of the self-organising system, that can be controlled, tuned or changed by an applied external stimulus, like external electric/magnetic field, mechanical stress or irradiation by light of different wavelength [1–3]; the last is actually of extremely high interest for a number of practical applications [4–11]. Various structures and specific properties characteristic for the low-molar-mass LC materials can be stabilised by grafting them on the polymeric backbone while designing the macromolecular structures. During last decades, self-assembling materials with desired functionality represent a fascinating area of intense research of the soft matter and liquid matter communities [5,12–16], which

CONTACT Alexej Bubnov bubnov@fzu.cz

provides a highlighted approach for the design of new material structures [17]. However, it is quite difficult to predict and keep under control the properties of the self-assembling materials [18–20]. One of the most exciting classes of organic materials that is able to self-assemble at nanoscopic length scale are those exhibiting the LC behaviour which can be tuned by the light illumination.

While designing new photosensitive LC materials, different photosensitive moieties [21] can be used for the material design: (i) the azobenzene group [21–23]; (ii) spiropyran group [21,24]; (iii) cinnamoyl group [21,25–28]; (iv) stilbene group [21,29–31]; coumarine group [21,32–34], etc. However, the difference in the chemical structure of photoactive moieties influences much their further post-isomerisation and the resulting properties, and, hence their functionality. For instance, photoalignment processes [35] play a crucial role for azobenzene, coumarin and cinnamoyl derivatives [36]. Utilisation of different photochromic gelators [36] allows the design and preparation of photochromic LC gels with fascinating optical properties and offers the pathways for the control over these properties by variation of the external electric field. Recently, the possible use of high-molecular-mass and low-molecular-mass photochromic compounds as gelators for low-molecular-mass nematic and cholesteric liquid crystals has been presented [37,38]. Systematic search for efficient gelators (such as low-molecular-mass and polymeric azobenzene and cinnamoyl derivatives) has been performed for different low-molecular-mass liquid crystals derived from of cyanobiphenyl, cyclohexane, etc. [36].

Generally, the azobenzene-based LCs combine the unique molecular self-organisation characteristic of liquids crystals with the exceptional light-induced response (molecular photo-alignment) of the azobenzene groups [39]. While azobenzene containing high-molecular-mass [39–41] and low-molecular-mass [22,42,43] photosensitive LC materials of various structure and functionality are intensively designed and investigated [39,44–46] and are even actively used for practical purposes like photoalignment [47]; high-density (volume or 3D) optical data storage devices [48] and other applications [49–51]. Nevertheless, the organic self-assembling materials containing cinnamoyl or other photosensitive moieties are much less considered [52–54]. Light-induced structural chemical transformations in photoactive LC compounds are also very highlighted and desirable. That is why the design and synthesis of new reactive mesogens, especially based on unconventional cinnamoyl group, still remains an actual and highlighted topic. Recently, the photosensitive functional cinnamoyl group has been used for the design LC materials of various shapes, like chiral [55–57] rod-like compounds but also for the discotic [58] and bent-shaped [59–61] LC materials. There are furthermore few cases, when the cinnamoyl group is used for the design of reactive monomers [39,57] and for further grafting them as a side-chain on the polyacrylate or polymethacrylate backbones.

Cinnamoyl moiety can also be used as a reactive terminal group that can undergo crosslinking reactions when subjected to heat or light [52,62]. The possibility to control the optical and electrical properties of reactive mesogens by aligning and fixing them using various methods enable their utilisation for special optical films [63], which can be widely used in both display and non-display applications, owing to the optical anisotropy of the liquid crystal structures [64]. The functional double bond of the cinnamic group [65] is well known for exhibiting a photo-induced isomerisation upon the UV irradiation, which can be used for inducing a surface anisotropy to achieve appropriate alignment of LC materials [65–69]. Using the cinnamic group, while designing new functional compounds, allows to achieve new luminescent LC materials with different emitting colour, which assure intense fluorescence in solution/solid-state and, simultaneously an appropriate LC behaviour [70].

The ***main objective*** of the present work is to design new cinnamoyl-based reactive mesogens with polymerisable vinyl group and to study their properties in order contribute to better understanding of molecular structure – mesomorphic property relationship for functional photosensitive reactive mesogens capable for both the photoisomerisation and photocycloaddition which can be further used for design of smart self-assembling macromolecular materials [36,71–75].

2. Experimental

This section contains of the detailed description of the synthetic route for the newly designed cinnamoyl-based reactive mesogens as well as the description of the experimental techniques used for the studies.

2.1. Synthesis of cinnamoyl-based reactive mesogens

General structure of the designed cinnamoyl-based reactive mesogens is presented in Figure 1. The molecular structure of the reactive mesogens differs in the number of carboxyl units and branching of chain linked to the mesogen's core by the carboxylic group.

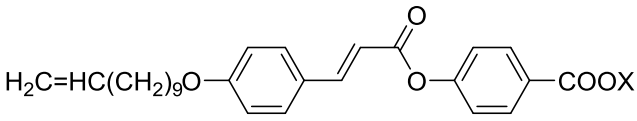

Figure 1. General chemical structure of the designed cinnamoyl-based reactive mesogens: the materials are denoted as: **USHM** for X=$C(CH_3)_2COOC_6H_{13}$; **USHG** for X=$CH_2COOC_6H_{13}$ and **USH 6** for X=C_6H_{13}.

Reactive mesogens were synthesised according to the synthetic routes shown in Figure 2. Commercial 10-undecenol **1** was converted to tosylate **2**, which was used for alkylation of 4-hydroxybenzaldehyde **3**. Alkylated aldehyde was then transformed to cinnamic acid **4** via Knoevenagel reaction with malonic acid. Aliphatic ester intermediates **6** and **8** were synthesised from hexane-1-ol by direct acylation (in the case of **6**) or esterification reaction (in the case of **8**). Analogously, hydroxy-ester **10a** was synthesised by direct esterification of 4-hydroxybenzoic acid **9** with hexane-1-ol. Alkylative esterification of 4-hydroxybenzoic acid **9** by hexyl chloroacetate **6** provided hydroxy-ester **10b**. In the case of the hydroxy-ester **10c**, the hydroxy group of 4-hydroxybenzoic acid **9** was first protected by the reaction with methyl chloroformate and then the resulting protected acid was transformed to benzoyl chloride **11** using thionyl chloride. In the next step benzoyl chloride **11** was esterified with hexyl 2-hydroxyisobutyrate **8** in pyridine and then the methoxycarbonyl-protective group was cleaved by aqueous ammonia giving hydroxy-ester **10c**. In the final step of the synthesis, the acid **4** and hydroxy-esters **10a-c** were reacted in the DCC-coupling reaction to yield target reactive mesogens **USH 6, USHG** and **USHM**.

Structure of all synthesised materials and intermediates were confirmed by NMR spectra recorded on Varian VNMRS 300 instrument; deuteriochloroform ($CDCl_3$) and hexadeuteriodimethyl sulphoxide

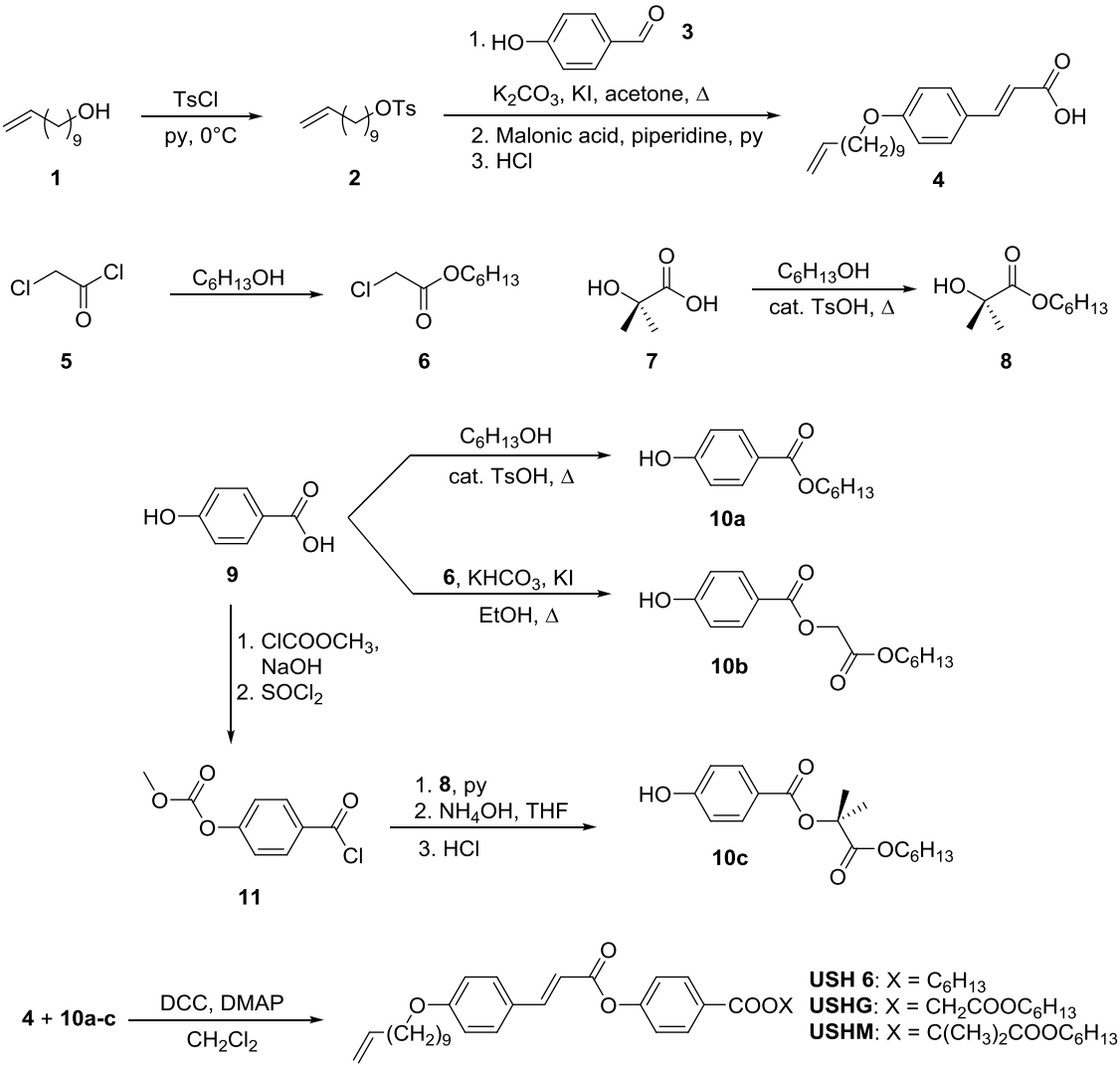

Figure 2. Synthetic route leading to target photosensitive cinnamoyl-based reactive mesogens.

(DMSO-d_6) were used as solvents and signals of the solvent served as the internal standard. In the following synthetic procedures' description, the chemical shifts (δ) are given in ppm and *J* values are given in Hz. The chemical purity of all materials and intermediates was checked by high-performance liquid chromatography (HPLC), which was carried out using a silica gel column (Biosphere Si 100–5 µm, 4x250, Watrex). The chemical purity was found between 99.5% and 99.7%.

Undec-10-enyl p-toluenesulfonate **2**

Undec-10-enyl *p*-toluenesulfonate **2** was synthesised following the procedure described in ref [76]. Starting from 10-undecenol (23.0 g, 0.14 mol) 42.0 g, (95%) of tosylate **2** was obtained. The product was used immediately in the next reaction without further purification. ^{1}H NMR ($CDCl_3$): 7.79 (2H, d, ArH), 7.34 (2H, d, ArH), 5.70–5.9 (1H, m, CH=), 4.76–5.10 (2H, m, C**H**$_2$=CH), 4.01 (2H, t, CH_2O), 2.05 (2H, dt, CH_2CH), 1.80 (2H, m, C**H**$_2CH_2O$), 1.30–1.60 (12H, m, $(CH_2)_6$).

4-(Undec-10-enyloxy)cinnamic acid **4**

A mixture of undec-10-enyl *p*-toluenesulfonate (6.50 g, 20.0 mmol), 4-hydroxy-benzaldehyde (3.30 g, 19.86 mmol), anhydrous potassium carbonate (5.50 g, 39.79 mmol), and acetone (100 ml) was heated under reflux for 10 h. The cooled mixture was added to water (300 ml), extracted with diethylether (3 × 70 ml), and the combined organic layers washed with water (2 × 70 ml) and dried over anhydrous magnesium sulphate. After removal of the solvent under reduced pressure, the residue was purified by crystallisation from hexane. Solid 4-(10-undecenyloxy)benzaldehyde was added to the solution of malonic acid (2.30 g, 21.55 mmol) in dry pyridine (15 ml) and piperidine (0.5 ml) was then added. The resulting mixture was refluxed with stirring for ca. 6 h (until CO_2 evolution stopped). Cooled mixture was poured into ice-cooled hydrochloric acid (1:2, 100 ml). The crude product was filtered off, washed with cold water, dried and then crystallised from ethanol to yield acid **4** (5.56 g, 88%). ^{1}H NMR ($CDCl_3$): 7.75 (1H, d, *J*=15.9, Ar-CH=), 7.50 (2H, d, *J*=8.6, H-2, H-6), 6.90 (2H, d, *J*=8.6, H-3, H-5), 6.32 (1H, d, *J*=15.9,=CHCOO), 5.70–5.9 (1H, m, CH=), 4.76–5.10 (2H, m, C**H**$_2$=CH), 4.0 (2H, t, *J* = 6.5, CH_2O), 2.23 (3H, s, $ArCH_3$), 1.97–2.09 (2H, m, C**H**$_2$CH=), 1.68–1.73 (2H, m, C**H**$_2CH_2O$), 1.33–1.68 (12H, m, $(CH_2)_6$).

Hexyl 2-chloroacetate **6**

According to Ref. [76]: Hexan-1-ol (10.20 g, 0.10 mol) was added dropwise with stirring to 2-chloroacetyl chloride (11.29 g, 0.10 mol). After stirring for 1 h the resulting mixture was distilled under reduced pressure (80–83°C/5 Torr). Yield was 14.6 g (81%). ^{1}H NMR ($CDCl_3$): 4.10–4.30 (3H, m, CH_2Cl, $COOCH_2$), 1.65 (2H, quin. *J* = 7.1, $COOCH_2C$**H**$_2$), 1.20–1.39 (6H, m, 3 × CH_2), 0.89 (3H, t, *J* = 6.7, CH_2C**H**$_3$).

Hexyl 2-hydroxy-2-methylpropanoate **8**

The mixture of 2-hydroxy-2-methylpropanoic acid (50.0 g, 0.48 mol), hexan-1-ol (48.0 g, 0.47 mol) and small amount of *p*-toluensulfonic acid in toluene (200 ml) was refluxed using Dean–Stark apparatus for 16 h during which portions of formed water were separated. After cooling, the resulting mixture was diluted with diethylether (500 ml) and washed with aqueous sodium hydroxide (150 ml, 10%), water and brine. Separated organic layer was dried over anhydrous magnesium sulphate. After removal of the solvent, crude product was distilled under reduced pressure (84°C/4 Torr). The yield was 74.28 g (83%). ^{1}H NMR ($CDCl_3$): 4.17 (2H, t, *J* = 7.0, CH_2O), 1.60 (2H, quin. *J*= 7.1, $COOCH_2C$**H**$_2$), 1.44 (6H, s, $C(CH_3)_2$), 1.21–1.41 (6H, m, 3 × (CH_2)), 0.86 (3H, t, *J* = 6.7, CH_2C**H**$_3$).

Hexyl 4-hydroxybenzoate **10a**

The mixture of 4-hydroxybenzoic acid (10.10 g, 72.0 mmol), octanol (19.0 g, 0.15 mol) and *p*-toluensulfonic acid (0.15 g, 0.9 mmol) in toluene (200 ml) was refluxed in Dean–Stark apparatus for 48 h during which portions of formed water were separated. After cooling, the resulting mixture was diluted with water (200 ml), neutralised with solution of potassium carbonate. Organic layer was separated and aqueous layer extracted with diethylether (2 × 150 ml). Collected organic layers were washed with water (100 ml), brine (100 ml) and dried over anhydrous magnesium sulphate. After evaporation of the solvent, crude hexyl 4-hydroxybenzoate was crystallised from hexane. Yield 14.10 g (88%), m.p. 51–52°C. ^{1}H NMR ($CDCl_3$): 7.96 (2H, d, *J* = 8.4, H-2, H-6), 6.88 (2H, d, *J* = 8.4, H-3, H-5), 6.19 (1H, s, OH), 4.29 (2H, t, *J* = 6.9, OCH_2), 1.76 (2H, m, OCH_2C**H**$_2$), 1.30–1.45 (6H, m, 3 × CH_2), 0.88 (3H, t, *J* = 6.6, CH_3).

2-(Hexyloxy)-2-oxoethyl 4-hydroxybenzoate **10b**

4-Hydroxybenzoic acid (17.0 g, 0.12 mol) was dissolved in ethanol (250 ml) and potassium bicarbonate (12.60 g, 0.13 mol) was added with intensive stirring. To this solution, hexyl 2-chloroacetate (20.0 g, 0.11 mol) was added dropwise and the mixture was refluxed for 4 h. After cooling, the resulting mixture was diluted in dichloromethane (400 ml), washed with water (2 × 150 ml) and dried over anhydrous magnesium sulphate. The solvent was removed under reduced pressure and the residue distilled (220°C/0.5 Torr). The yield was 26.20 g (77%). ^{1}H NMR ($CDCl_3$): 7.91 (2H, d, *J* = 8.5, H-2, H-6), 6.87 (1H, br. s., OH), 6.81 (2H, d, *J* = 8.5, H-3, H-5), 4.85 (2H, s, *J* = 7.1, OCH_2COO), 4.22 (2H, t, *J* = 6.4, $COOCH_2$), 1.67 (2H, quin. *J* = 7.1, $COOCH_2C$**H**$_2$), 1.21–1.35 (6H, m, $(CH_2)_3$), 0.88 (3H, *J* = 6.7, CH_2C**H**$_3$).

4-(Methoxycarbonyoxy)benzoyl chloride **11**

4-hydroxybezoic acid (27.60 g, 0.20 mol) was dissolved in a mixture of sodium hydroxide (20.0 g, 0.50 mol) and water (300 ml) and cooled to 0°C. Then, methyl chloroformate (28.30 g, 0.30 mol) was added dropwise with stirring, keeping the temperature at 0°C. The reaction mixture was then stirred for ca. 2 h while a white precipitate was gradually formed. Resulting mixture was acidified by a small amount of hydrochloric acid (pH 4–5) and white solid was filtered off and washed with cold water. After drying, the solid was recrystallised from ethanol and dried under vacuum. Obtained 4-(methoxycarbonyloxy)benzoic acid was suspended in thionyl chloride (40 ml) and a catalytic amount of DMF was added. The reaction mixture was refluxed for 2 h. The excess of thionyl chloride was distilled off. Oily residue was diluted with toluene and the solvent removed on rotatory evaporator. Obtained benzoyl chloride **11** was used in the next synthetic step without further purification. ^{1}H NMR ($CDCl_3$): 8.18 (2H, d, *J* = 8.8, H-2, H-6), 7.37 (2H, d, *J* = 8.8, H-3, H-5), 3.96, (3H, s, OCH_3).

1-(Hexyloxy)-2-methyl-1-oxopropan-2-yl 4-hydroxybenzoate **10c**

Benzoyl chloride **11** (10.0 g, 46.60 mmol) dissolved in toluene (50 ml) was added dropwise to the stirred mixture of **8** (8.50 g, 45.15 mmol) and dry pyridine (8 ml) in toluene (100 ml). The reaction mixture was stirred for 6 h and then refluxed for 30 min. Resulting cooled mixture was filtered and the filtrate washed with diluted hydrochloric acid (100 ml, 5%) and water (100 ml). Separated organic layer was dried with anhydrous magnesium sulphate. After evaporation of solvent on rotavap, the residue was dissolved in tetrahydrofurane (150 ml) and cooled to −20°C. To this precooled solution, concentrated aqueous ammonia (25 ml, 25%, 0.16 mol) was added with stirring. The reaction mixture was stirred and let warm to room temperature and the progress of the hydrolysis was monitored by TLC. After ca. 45 min the resulting mixture was poured into water (200 ml) and neutralised with hydrochloric acid. The organic layer was separated and the aqueous layer extracted with diethylether (2 × 70 ml). Combined organic layers were washed with water (70 ml) and dried over anhydrous sodium sulphate. The solvent was removed on rotavap and the oily residue purified by chromatography on silica (dichloromethane-acetone (97:3)). Yield 11.10 g (81%) of viscous liquid **10c**. ^{1}H NMR ($CDCl_3$): 7.89 (2H, d, *J* = 8.8, H-2, H-6), 6.84 (2H, d, *J* = 8.8, H-3, H-5), 4.15 (2H, t, *J* = 6.7, $COOC\mathbf{H}_2$), 1.68 (6H, s, $(C\mathbf{H}_3)_2C$), 1.60 (2H, quin. *J* = 7.0, $COOCH_2C\mathbf{H}_2$), 1.10–1.43 (6H, m, 3 × CH_2), 0.88 (3H, *J* = 6.7, $CH_2C\mathbf{H}_3$), ^{13}C NMR ($CDCl_3$): 173.38 (s, C-**C**OO), 165.51 (s, ArCOO), 160.89 (s, C-4), 131.97 (s, C-2, C-6), 121.68 (s, C-1), 115.20 (s, C-3, C-5), 78.38 (s, **C**-COO), 65.65 (s, $\mathbf{C}H_2OOC$), 31.26 (s, $\mathbf{C}H_2CH_2CH_3$), 28.30 (s, $\mathbf{C}H_2CH_2O$), 25.41 (s, $\mathbf{C}H_2(CH_2)_2O$), 24.71 (s, $(\mathbf{C}H_3)_2C$), 22.42 (s, $\mathbf{C}H_2CH_3$), 13.90 (s, $CH_2\mathbf{C}H_3$).

(E)-hexyl 4-((3-(4-(undec-10-en-1-yloxy)phenyl)acryloyl)oxy)benzoate (**USH 6**)

Benzoic acid **4** (2.0 g, 6.32 mmol) and phenol **12a** (1.40 g, 6.28 mmol) were dissolved in dry dichloromethane (50 ml) and dicyclohexylcarbodiimide (1.37 g, 6.63 mmol) and 4-(*N*,*N*-dimethylamino)pyridine (0.15 g, 1.75 mmol) were added. The mixture was stirred for 24 h and then the precipitated dicyclohexylurea was filtered off. Resulting filtrate was evaporated and further purified by column chromatography on silica (eluent dichloromethane-acetone 99.8:0.2) and crystallised from hexane. The yield was 2.65 g (81%) of **USH 6** compound.

^{1}H NMR ($CDCl_3$): δ 8.20 (d, 2H, *J* = 8.6H-2′, H-6′), 7.85 (1H, d, *J* = 15.8, Ar-CH=), 7.55 (2H, d, *J* = 8.8, H-2, H-6), 7.34 (d, 2H, J = 8.6, H-3′, H-5′), 6.94 (2H, d, *J* = 8.8, H-3, H-5), 6.49 (2H, d, *J* = 15.8,=CHCOO), 5.70–5.92 (m, 1H, CH=), 4.90–5.10 (1H, m, $C\mathbf{H}{=}CH_2$), 4.30 (t, 2H, *J* = 6.5, CH_2OOC) 4.09 (t, 2H, *J* = 6.7, CH_2O), 1.98–2.10 (m, 2H, $C\mathbf{H}_2CH{=}$), 1.68–1.89 (m, 4H, 2 × $C\mathbf{H}_2CH_2O$), 1.20–1.69 (m, 18H, 9 × CH_2), 0.90 (t, 3H, *J* = 6.7, $C\mathbf{H}_3CH_2$). ^{13}C NMR ($CDCl_3$): 165.19 (s, CH**C**OO), 164.81(s, ArCOO), 161.49 (s, C-4), 155.89 (s, C-4′), 147.11 (s, ArCH), 139.18 (s, $\mathbf{C}H{=}CH_2$), 130.88 (s, C-2′, C-6′), 130.11 (s, C-2, C-6), 126.50 (s, C-1), 126.43 (s, C-1′), 121.80 (s, C-3′, C-5′), 114.89 (s, C-3, C-5), 114.13 (s, $\mathbf{C}H_2{=}CH$), 113.74 (s, **C**H=COO), 68.20 (s, $ArOCH_2$), 65.50 (s, $COO\mathbf{C}H_2$), 33.78 (s, $\mathbf{C}H_2CH{=}CH_2$), 31.31 (s, $\mathbf{C}H_2CH_2CH_3$), 29.05–29.48 (m, 5 × CH_2), 28.85 (s, $\mathbf{C}H_2CH_2O$), 28.41 (s, $\mathbf{C}H_2CH_2O$), 25.95 (s, $\mathbf{C}H_2(CH_2)_2O$), 25.42 (s, $\mathbf{C}H_2(CH_2)_2O$), 22.49 (s, $\mathbf{C}H_2CH_3$), 13.98 (s, $CH_2\mathbf{C}H_3$). Elemental Analysis for $C_{33}H_{44}O_5$ (520.71): calc. C 76.12, H 8.52; found C 77.20, H 8.59.

(E)-2-(hexyloxy)-2-oxoethyl 4′-((3-(4-(undec-10-en-1-yloxy)phenyl)acryloyl)oxy)benzoate (**USHG**)

The target **USHG** compound was synthesised using the same DCC-coupling procedure described for **USH 6** compound. The reaction of benzoic acid **4** (1.50 g, 4.74 mmol) and phenol **10b** (1.33 g, 4.74 mmol) in the presence of DCC (1.0 g, 4.85 mol) and DMAP (0.15 g, 1.75 mmol) resulted in the crude product and after column chromatography (eluent dichloromethane-acetone 99.8:0.2) and crystallisation from hexane yielded of 2.44 g (89%) of **USHG**. ^{1}H NMR ($CDCl_3$): 8.16 (2H, d, *J*= 8.8, H-2′, H-6′), 7.85 (1H, d, *J* = 15.8, Ar-CH=), 7.55 (2H, d, *J* = 8.8, H-2, H-6), 7.29 (2H, d, *J* = 8.8, H-3′, H-5′), 6.94 (2H, d, *J* = 8.8, H-3, H-5), 6.49

(2H, d, J = 15.8,=CHCOO), 5.68–5.95 (2H, m, C**H**$_2$ =CH), 4.90–5.09 (1H, m, C**H**=CH$_2$), 4.86 (2H, s, OCH$_2$COO), 4.20 (2H, t, J = 6.7, COOCH$_2$), 4.01 (2H, t, J = 6.5, OCH$_2$), 1.94–2.16 (2H, m, C**H**$_2$CH=), 1.74–1.91 (2H, m, C**H**$_2$CH$_2$O), 1.61–1.72 (2H, m, C**H**$_2$ CH$_2$O), 1.15–1.55 (18H, m, 9 × CH$_2$), 0.89 (3H, J = 6.7, C**H**$_3$CH$_2$). ^{13}C NMR ($CDCl_3$): 167.83 (s, CH$_2$**C**OO), 165.22 (s, CH**C**OO), 165.10 (s, ArCOO), 161.53 (s, C-4), 154.99 (s, C-4′), 147.10 (s, ArCH), 139.18 (s, **C**H=CH$_2$), 131.50 (s, C-2′, C-6′), 130.14 (s, C-2, C-6), 126.49 (s, C-1), 126.43 (s, C-1′), 121.80 (s, C-3′, C-5′), 114.93 (s, C-3, C-5), 114.13 (s, **C**H$_2$=CH), 113.75 (s, **C**H=COO), 68.18 (s, ArOCH$_2$), 65.48 (s, COO**C**H$_2$), 61.23 (s, **C**H$_2$COO), 33.78 (s, **C**H$_2$CH=CH$_2$), 31.31 (s, **C**H$_2$CH$_2$CH$_3$), 29.09–29.47 (m, 5 × CH$_2$), 28.89 (s, **C**H$_2$ CH$_2$O), 28.42 (s, **C**H$_2$CH$_2$O), 25.96 (s, **C**H$_2$(CH$_2$)$_2$O), 25.43 (s, **C**H$_2$(CH$_2$)$_2$O), 22.48 (s, **C**H$_2$CH$_3$), 13.97 (s, CH$_2$**C**H$_3$). Elemental Analysis for $C_{35}H_{46}O_7$ (578.75): calc. C 72.64, H 8.01; found C 73.78, H 8.10.

(E)-1-(hexyloxy)-2-methyl-1-oxopropan-2-yl 4′-((3-(4-(undec-10-en-1-yloxy)phenyl)acryloyl)oxy)benzoate (**USHM**)

The target **USHM** compound was synthesised using the same DCC-coupling procedure described for **USH 6** compound. The reaction of benzoic acid **4** (1.50 g, 4.74 mmol) and phenol **10c** (1.46 g, 4.73 mmol) in the presence of DCC (1.0 g, 4.85 mol) and DMAP (0.15 g, 1.75 mmol) resulted in the crude product which was purified by column chromatography on silica (eluent dichloromethane-acetone 99.8:0.2) and recrystallised from hexane. Yield 2.43 g (85%) of **USHM**. ^{1}H NMR ($CDCl_3$) 8.10 (2H, d, J = 8.6, H-2′, H-6′), 7.85 (1H, d, J = 15.8, Ar-CH=), 7.54 (2H, d, J = 8.8, H-2, H-6), 7.26 (2H, d, J = 8.6, H-2′, H-6′), 6.94 (2H, d, J = 8.8, H-3, H-5), 6.49 (2H, d, J = 15.8,=CHCOO), 5.68–5.95 (2H, m, C**H**$_2$=CH), 4.86–5.10 (1H, m, C**H**=CH$_2$), 4.15 (2H, t, J = 6.7, COOCH$_2$), 4.01 (2H, t, J = 6.5, OCH$_2$), 1.96–2.19 (2H, m, C**H**$_2$CH=), 1.74–1.89 (2H, m, C**H**$_2$CH$_2$O), 1.70 (6H, s, C(CH$_3$)$_2$), 1.53–1.67 (2H, m, C**H**$_2$CH$_2$O), 1.13–1.52 (18H, m, 9 × CH$_2$), 0.85 (3H, J = 6.7, C**H**$_3$ CH$_2$). ^{13}C NMR ($CDCl_3$): 172.59 (s, C-**C**OO), 165.16 (s, CH**C**OO), 164.65 (s, ArCOO), 161.52 (s, C-4), 154.73 (s, C-4′), 147.03 (s, ArCH), 139.18 (s, **C**H=CH$_2$), 131.27 (s, C-2′, C-6′), 130.13 (s, C-2, C-6), 127.45 (s, C-1′), 126.45 (s, C-1), 121.65 (s, C-3′, C-5′), 114.94 (s, C-3, C-5), 114.14 (s, **C**H$_2$=CH), 113.82 (s, **C**H=COO), 78.87 (s, **C**(CH$_3$)$_2$), 68.18 (s, ArOCH$_2$), 65.48 (s, COO**C**H$_2$), 33.79 (s,**C**H$_2$CH=CH$_2$), 31.30 (s, **C**H$_2$CH$_2$CH$_3$), 29.04-29.55 (m, 5 × CH$_2$), 28.90 (s, **C**H$_2$CH$_2$O), 28.36 (s, **C**H$_2$ CH$_2$O), 25.97 (s, **C**H$_2$(CH$_2$)$_2$O), 25.46 (s, **C**H$_2$(CH$_2$)$_2$O), 24.71 (s, **C**(CH$_3$)$_2$), 22.47 (s, **C**H$_2$CH$_3$), 13.94 (s, CH$_2$ **C**H$_3$). Elemental Analysis for $C_{37}H_{50}O_7$ (606.80): calc. C 72.62, H 8.31; found C 73.86, H 8.42.

2.2. Experimental techniques

Sequence of mesophases was determined by the observation of characteristic textures and their changes in the polarising optical microscope (POM) – Nikon Eclipse E600POL (Nikon, Tokyo, Japan). Planar cells (bookshelf geometry) of 12 μm thickness (glasses with ITO transparent electrodes (5 × 5 mm^2)) were supplied by Military University of Technology (Warsaw, Poland). The cells were filled with studied reactive mesogens in the isotropic phase by means of capillary action. For texture observation on samples with homeotropic alignment, i.e. free-standing films (FSF) have also been used; while preparing the FSF, the liquid-crystalline material was mechanically spread over a circular hole (diameter 3 mm) in a metal plate placed in the hot stage. The Linkam LTS E350 (Linkam, Tadworth, UK) heating/cooling stage with a TMS 93 temperature programmer was used for the temperature control, which enabled temperature stabilisation within ±0.1 K. The phase transition temperatures were determined by differential scanning calorimetry (DSC) using Perkin-Elmer DSC8000 calorimeter (PerkinElmer, Shelton, CT, USA). The samples of about 4–8 mg, hermetically sealed in aluminium pans, were placed into the calorimeter chamber filled with nitrogen. For the evaluation of the phase transition temperatures the calorimetric measurements were performed on cooling/heating runs at a rate of 5 K min^{-1}. For the study of the kinetics of the phase transition temperatures, heating/cooling rates of (1, 2, 3, 5, 10, 20, 30, 40, 50) K min^{-1} have been used. Temperature and enthalpy change values were calibrated on the extrapolated onset temperatures and the enthalpy changes of the melting points of water, indium and zinc.

Small and wide-angle X-ray scattering (SAXS and WAXS, respectively) measurements have been performed to determine the structural properties of the identified mesophases. For measurements in small-angle range (determination of the smectic layer spacing, d, e.g. the interlayer spacing) a Bruker D8 Discover system has been used (parallel beam of *CuKα* radiation formed by Goebel mirror, Anton Paar DCS 350 heating stage, scintillation detector) while wide-angle diffractograms have been obtained with a Bruker D8 GADDS system (parallel beam of *CuKα* radiation formed by Goebel mirror monochromator and point collimator, Vantec-2000 area detector, modified Linkam heating stage). In both systems, the temperature stability was 0.1 K. Samples were prepared in a form of thin film or droplet on a heated surface.

Solutions of reactive mesogen **USHG** in chloroform were irradiated by a UV-hand lamp (8 W sterilair BLB-8, 366 nm, Philips, China); the irradiation

conditions were as follows: wavelength 366 nm, 1.7 mW/cm^2, 30 min. Determination of final composition of the rod-like and cross-linked molecule 'mixtures' after irradiation was carried out using HPLC, which was carried out using a silica gel column (Kromasil Si 100–5 μm, 4 × 250 mm, Watrex) with a mixture of 99.9% of toluene and 0.1% of methanol as an eluent, and detection of the eluting products by a UV-VIS detector (λ = 290 nm).

3. Results and discussion

In this section, the experimental results obtained on newly designed cinnamoyl-based reactive mesogens are presented. The photosensitive behaviour of **USHG** reactive mesogen under UV irradiation in solution has been investigated. The LC behaviour of all three reactive mesogens was studied by POM and DSC. Representative study of the kinetics of the phase transition temperatures is presented for **USHG** reactive mesogen on heating and cooling runs. The structure of the mesophases was confirmed by SAXS and WAXS measurements. All the results are discussed in order to contribute to molecular structure – self-assembling behaviour relationship for this specific class of LC materials.

3.1. Photosensitive behaviour of USHG reactive mesogen under UV irradiation in solution

Cinnamates are known to undergo several photochemical processes under illumination by UV light of wavelengths higher than 300 nm (see Figure 3). These are *E-Z* isomerisation leading to bent-shaped *Z*-isomer, cyclisation (dimerisation) [77,78] giving up to eleven isomeric tetra-substituted cyclobutanes and finally the *photo*-Fries rearrangement giving a phenone derivative as product. In order to investigate the basic photochemical behaviour and the stability of our new cinnamate reactive mesogens, we decided to do the photochemical study in solution. The sole process observed in solution by both ^{1}H-NMR and HPLC analysis was *E-Z* isomerisation.

The results of the HPLC analysis for both studied materials at three different concentrations illuminated by UV light (366 nm) for 30 min are given in Table 1, in terms of residual rod-like *E*-isomer content. The low conversions of *E*-isomer to photoproducts is given by the concentration range used, at which the photochemical processes are clearly in the diffusion-controlled regime, despite the used wavelength of UV light is nearly at the absorption edge of the material (Figure 4). This is also evidenced by the smaller area of the photoproduct peak B in the chromatographs at higher concentrations (Figure 5). Since there was always

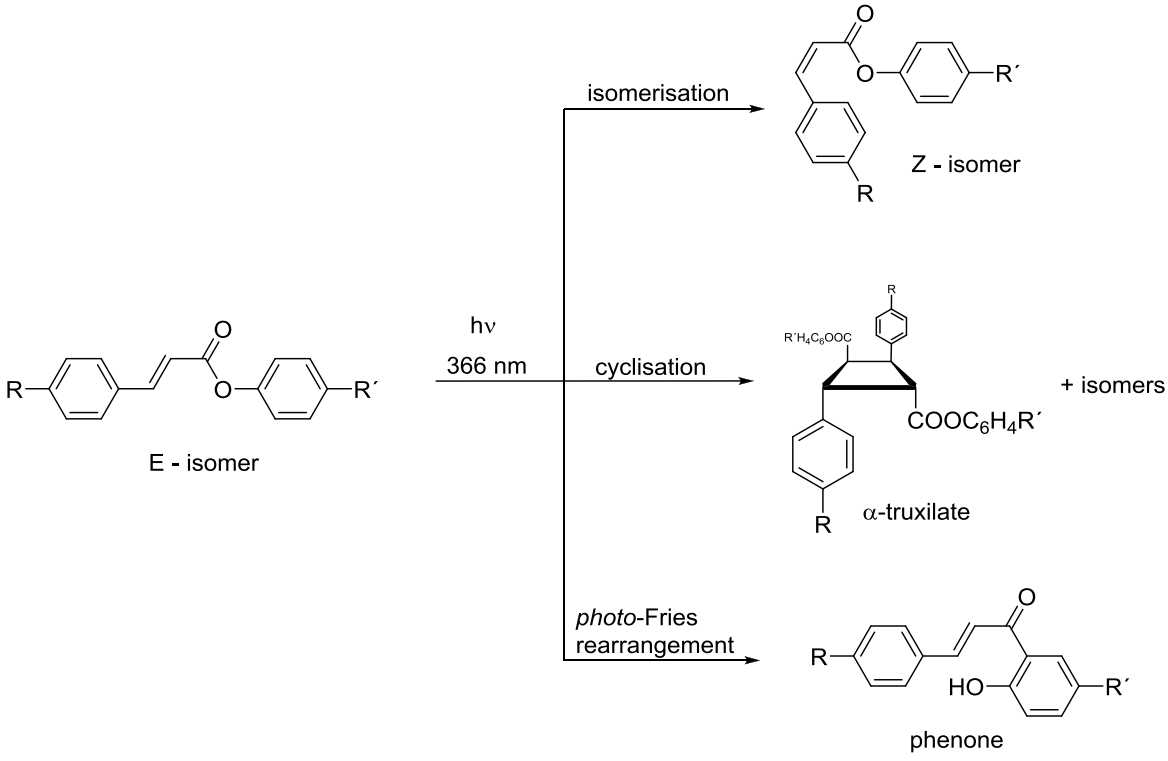

Figure 3. Possible photochemical reactions of studied cinnamates under UV irradiation.

Table 1. Data obtained on three different solutions for both **USHG** and **USHM** reactive mesogens in chloroform and the ratio of remaining rod-like *E*-isomer after irradiation by UV light (λ = 366 nm) for 30 min.

	Concentration in solution [mg/ml]	Remaining (*E*) rod-like compound [wt%]
USHGa	10.0	79.0
USHGb	50.0	87.0
USHGc	100.0	94.0
USHMa	10.0	88.0
USHMb	50.0	97.0
USHMc	100.0	98.0

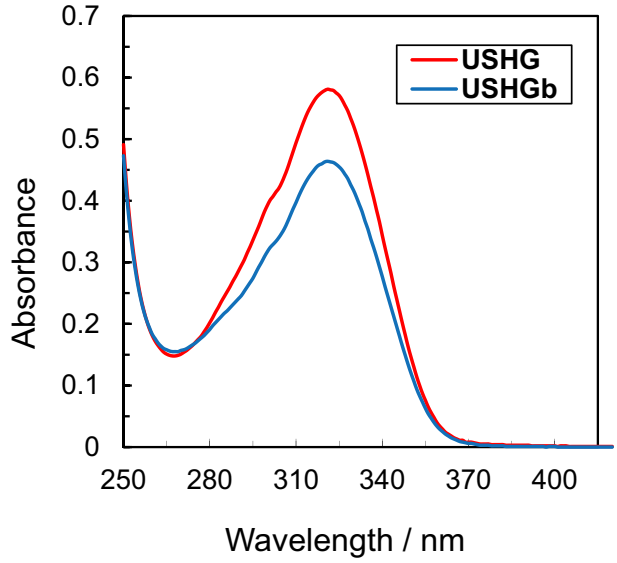

Figure 4. (Colour online) Difference of the absorbance spectra for original **USHG** reactive mesogen and the **USHGb** mixture of isomers obtained after irradiation by UV light (λ = 366 nm) during 30 min.

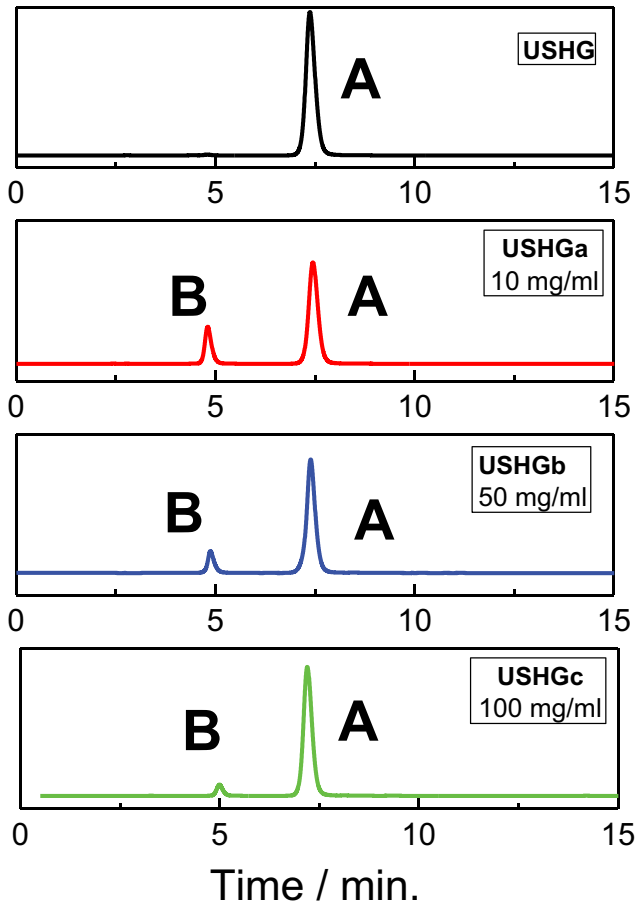

Figure 5. (Colour online) HPLC chromatograms for original (*E*)-**USHG** reactive mesogen and isomer mixtures obtained by irradiation of chloroform solutions **USHGa, USHGb** and **USHGc** by UV light (λ = 366 nm) for 30 min clearly show the presence of one photoproduct (peak B) and different ratio of (*E*)-**USHG** (peak A) in the isomer mixtures upon change of the concentration.

only one peak of product in the chromatograms obtained for all concentrations and illumination times (Figure 5), we can confirm, that there is only one photochemical reaction active in the solution of studied reactive mesogens. The same is suggested by the UV absorption curve of irradiated mixture (Figure 4), which has almost identical shape with the pure *E*-isomer, but at lower absorbance values due to the presence of *Z*-isomer which has lower extinction in this spectral region. It was confirmed by ^{1}H-NMR spectroscopy of the sample irradiated for 90 min, that only *E-Z* isomerisation was active for the studied materials under given experimental conditions (Figure 6). Absence of [2 + 2] cycloaddition in solution is a usual observation [79], since cycloaddition requires close proximity of the molecules and the molecules in the solution are rather isolated. Cycloaddition can be absent even in the solid phase. However, only in some special cases, like for example cinnamate-containing dendrimers, where the flexible spacer consisting of $(CH_2)_{10}$ groups located between the dendritic core and cinnamoyl groups may prevent [2 + 2] photocycloaddition, since this process is topochemically controlled [21].

More substantial observation is the absence of phenone product of *photo*-Fries rearrangement. It can be suggested that the electron withdrawing carboxylic group serving as a linker of the terminal chain can destabilise the phenoxyl radical intermediate of the *photo*-Fries rearrangement making it energetically disfavoured process. The absence of this reaction also indicates the high stability of these new reactive mesogens. However, only low power UV light of a wavelength at the absorption edge of the material was used; therefore, a study using a higher power of UV-light and a wavelength closer to absorption maximum of the material would be advantageous to make a robust decision on materials' stability.

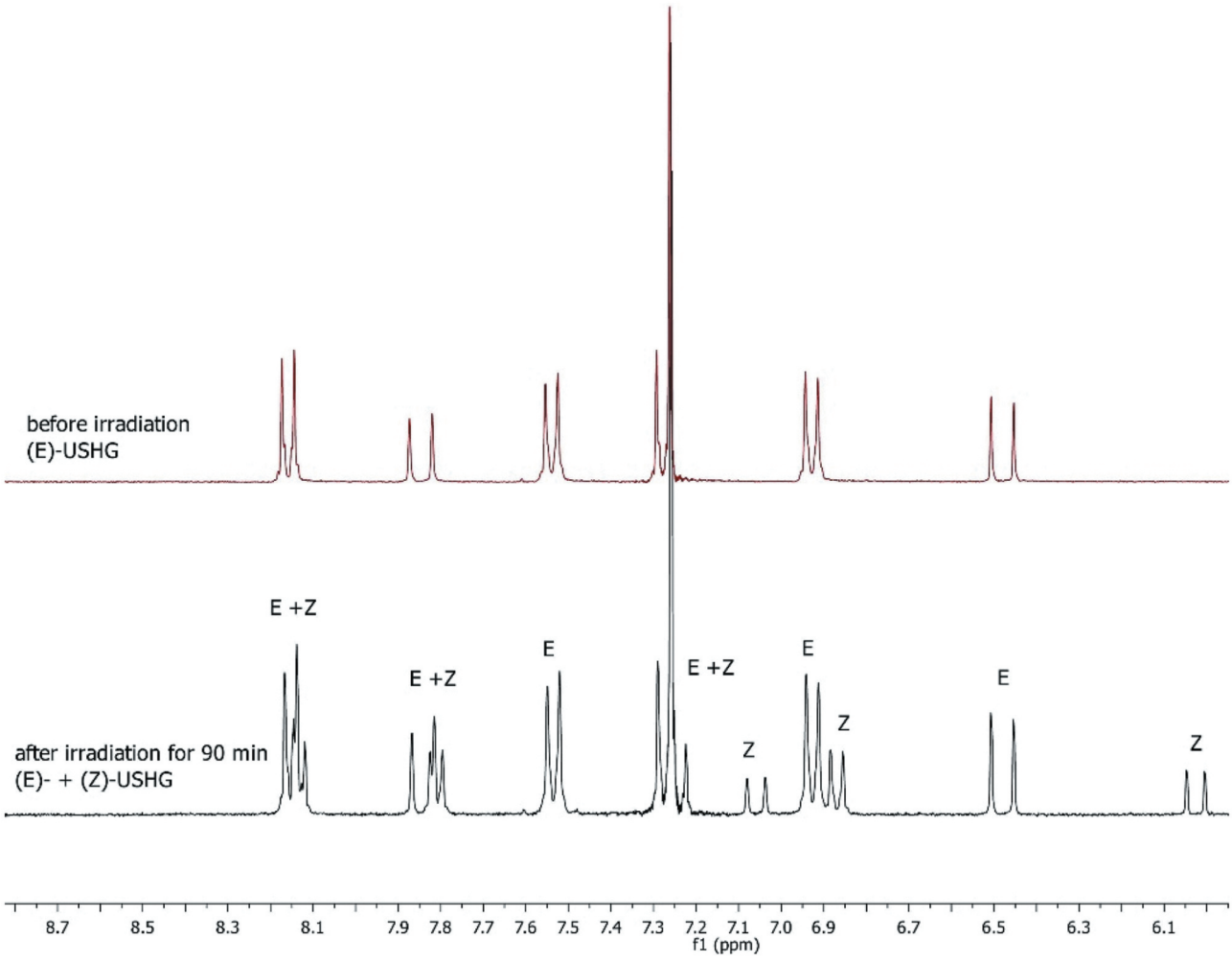

Figure 6. (Colour online) ^{1}H-NMR spectra of pure (*E*)-**USHG** and a mixture of isomers obtained by irradiation by UV light for 90 min.

3.2. Mesomorphic behaviour

For all the studied reactive mesogens, sequences of phases were determined by characteristic textures and their changes were observed in a POM. The phase transition temperatures and transition enthalpies were evaluated from DSC measurements. The LC properties of all compounds under study are summarised in Table 2. The **USHM** mesogen with the longest chain does not exhibit the LC behaviour. On cooling from the isotropic phase, the **USHG** reactive mesogen forms the nematic phase at ~97°C. On further cooling, the orthogonal smectic A (SmA) phase appears and, at about 70°C, the SmA-SmC phase transition takes place; this material crystallises (Cr – crystal phase) at about room temperature. However, due to quite high melting point, almost the whole temperature range of the SmC phase has monotropic character, which means that the mesophase is detected on cooling only. The reactive mesogen with the shortest chain (**USH 6**) shows the orthogonal SmA and the tilted SmC phases down to room temperature; below the melting point the SmC phase is monotropic

Table 2. Sequence of phases determined by POM; melting points, m.p. (°C) and clearing points c.p. (°C) measured on heating; phase transition temperatures (°C) measured on cooling (10 K min^{-1}) and respective enthalpy values ΔH (kJ/mol) determined by DSC for the studied reactive mesogens; '•' stands if the phase exist; '-' stands if the phase does not exist.

	m.p.	c.p.	Cr	T/ΔH	SmC	T/ΔH	SmA	T/ΔH	N	T/ΔH	Iso
USHM	50.8 [+24.6]	50.8 [+24.6]	•	18.9 [−4.3]	-		-		-		•
USHG	67.1 [+43.5]	98.6 [+1.3]	•	25.8 [−3.9]	•	69.9 [−0.06]	•	93.6 [−1.0]	•	96.6 [−1.4]	•
USH 6	50.2 [+31.3]	100.3 [+5.3]	•	32.2 [−16.5]	•	75.2 [−0.1]	•	94.7 [−5.0]	-		•

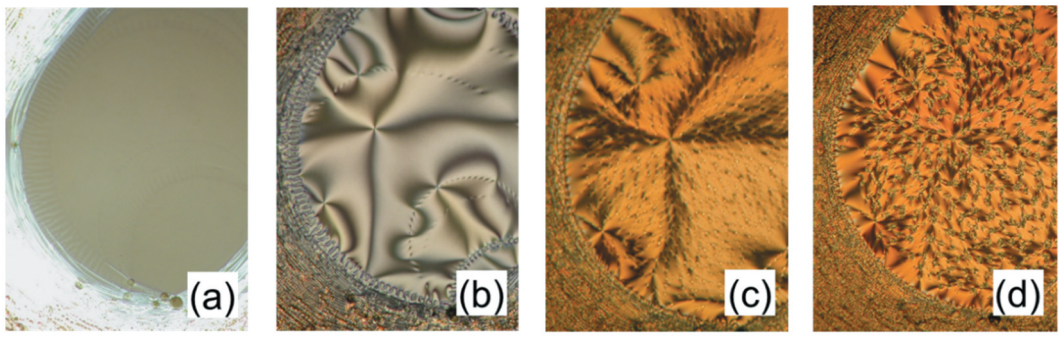

Figure 7. (Colour online) Microphotographs of characteristic textures obtained in the POM on free-standing films of **USH 6** material (homeotropic orientation): (a) the orthogonal SmA phase at 85°C; (b) the tilted SmC phase at 74°C; (c) the SmC phase at 40°C; (d) the SmC-crystal phase transition at 32°C. Width of the photos is about 300 µm.

(see Table 2), similarly as for the **USHG** compound. The melting point of **USH 6** reactive mesogen is found to be considerably lower than that of the **USHG** mesogen.

Beyond the observation of the characteristic textures done on the planar samples, the FSF has been used. The homeotropic textures obtained on the FSF for **USH 6** reactive mesogen are shown on Figure 7, specifically the texture of the orthogonal SmA phase (Figure 7(a)), the schlieren textures of the tilted SmC phase at two temperatures as indicated (Figure 7(b,c)) and the SmC-Cr phase transition (Figure 7(d)). All the textures observed in POM on the FSF samples in homeotropic alignment were found to be very typical and characteristic for the detected mesophases.

3.3. Mesomorphic properties of mixtures after UV irradiation

As it has been described in section 3.1, several solutions were prepared and irradiated by UV light in order to check the effect of the solution concentration on the capability of the reactive mesogens for photoreactions. The LC behaviour of the materials obtained by removal of the solvent after UV irradiation has been carefully checked. The LC properties of all resulting mixtures containing isomers are summarised in Table 3. The melting and clearing points were found slightly lower than that for the non-irradiated **USHG** reactive mesogen owing to the presence of the non-mesogenic bent-shaped *Z*-isomer. However, it seems that presence of *Z*-isomer does not disrupt the nano-organisation of the molecules significantly, since the sequence of mesophases remains exactly the same as for the non-irradiated material; only a slight difference in phase transition temperatures has been found (see Table 3). All three resulting mixtures exhibit the nematic phase as well as the SmA and SmC phases.

The microphotographs of the characteristic textures for **USHGb** reactive mesogen (as an example) obtained on 12 mm thick samples in planar geometry are presented in Figure 8: the Iso-N phase transition appearing as a nematic droplet growth (Figure 8(a)); the classical fan-shaped texture of the SmA phase (Figure 8(b)) and the broken fan-shaped texture of the SmC phase (Figure 8(c)); the texture of the crystal phase is shown on Figure 8(d). The textures of the respective mesophases were found to be very similar for all the mixtures, namely for **USHGa, USHGb, USHGc**, if compared to the non-irradiated **USHG** reactive mesogen.

3.4. Kinetics of the phase transition temperatures

The kinetics of the phase transition temperatures has been checked using DSC measurements under several

Table 3. Sequence of phases determined by POM; melting points, m.p. (°C) and clearing points c.p. (°C) measured on heating; phase transition temperatures (°C) measured on cooling (10 K min^{-1}) and respective enthalpy values ΔH (kJ/mol) determined by DSC for samples after UV irradiation.

	m.p.	c.p.	Cr	T/ΔH	SmC	T/ΔH	SmA	T/ΔH	N	T/ΔH	Iso
USHG	67.1 [+43.5]	98.6 [+1.3]	•	25.8 [−3.9]	•	69.9 [−0.06]	•	93.6 [−1.0]	•	96.6 [−1.4]	•
USHGa	65.8 [+36.1]	91.8 [+0.06]	•	19.9 [−30.1]	•	54.5 [−0.01]	•	83.4 [−4.3]	•	88.6 [−0.01]	•
USHGb	66.1 [+35.8]	91.7 [+0.1]	•	30.5 [−31.8]	•	41.6 [−0.01]	•	77.5 [−3.9]	•	82.4 [−0.06]	•
USHGc	66.1 [+39.4]	92.9 [+0.3]	•	19.9 [−28.6]	•	46.6 [−0.06]	•	84.8 [−0.1]	•	88.7 [−0.1]	•

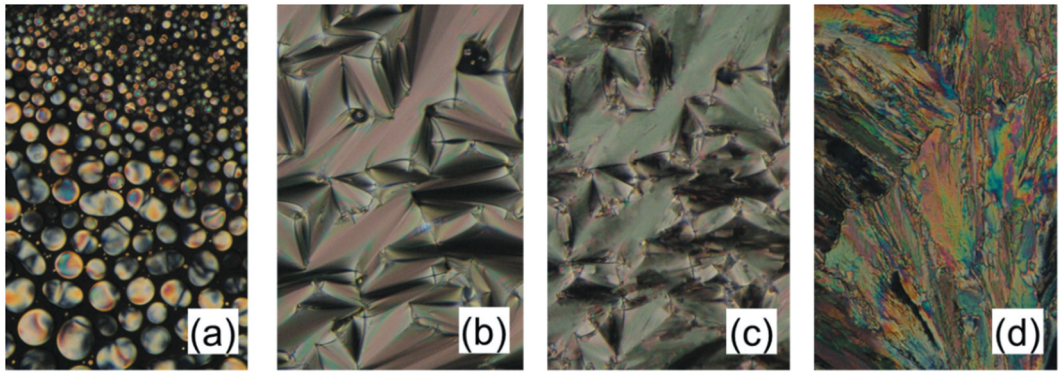

Figure 8. (Colour online) Microphotographs of characteristic textures obtained in the POM on planar samples of **USHGb** reactive mesogen: (a) the Iso-N phase transition at about 82°C; (b) the SmA phase at about 70°C; (c) the tilted SmC phase at about 39°C; (d) the crystal phase. Width of the photos is about 300 µm.

cooling rates, as presented in Figure 9. For this study, only data from the second cooling runs has been used. It has been found that the stability of all the mesophases slightly depends on the rate of cooling. While increasing the rate of cooling the Iso-N, N-SmA and SmA-SmC phase transition temperatures slightly decreases; the stability of the phases increases. However, the SmC-Cr phase transition shows a clear signs of super-cooling [80], being more pronounced especially at cooling rates higher than 20 K. This effect is also related to the monotropic character of the low-temperature range of the SmC phase.

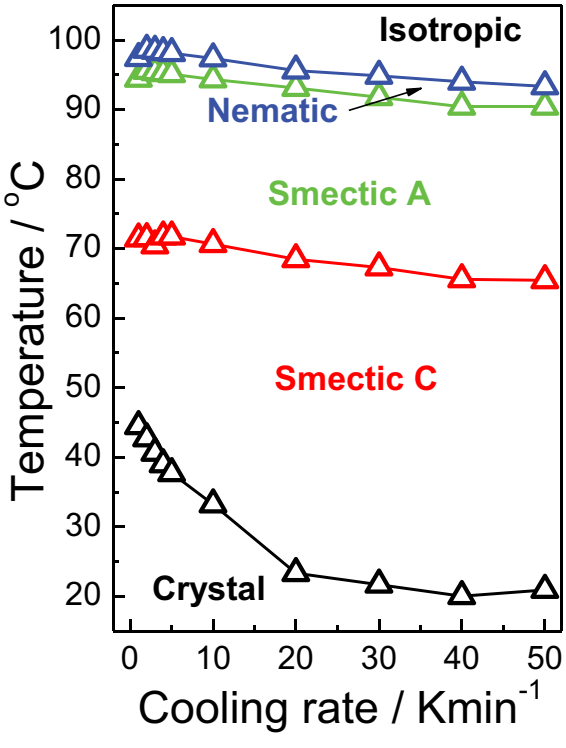

Figure 9. (Colour online) Phase diagram for the **USHG** reactive mesogen obtained on cooling runs indicating a clear difference of the phase transition temperatures on the DSC measurement rate.

3.5. X-ray study

Small and wide-angle X-ray scattering measurements have been performed to confirm the mesophases' identification and to determine their structural properties. The results of X-ray studies, namely the temperature dependence of the smectic layer spacing, d, are presented in Figure 10 for **USHG** and **USH 6** reactive mesogens (see Figure 10(a,c), respectively), and for one of the resulted **USHGa** mixture obtained after irradiation by UV light (see Figure 10(b)).

All studied materials exhibit a slight increase of d(T) values in the SmA phase on approaching the phase transition to the SmC phase. At the SmA-SmC phase transition, a typical decrease in d values starts, caused by the tilting of the molecules in the SmC phase. For **USHG** and **USH 6** reactive mesogens, on further cooling towards crystallisation, the layer spacing starts to increase due to stretching of the aliphatic terminal chains and/or due to increasing of the orientational order of molecules. The insets of Figure 10 show the respective WAXS data at the indicated temperatures. At high diffraction angles, there is a broad peak indicating the liquid order of the molecules within the smectic layers, which confirms identification of mesophases as liquid-like smectic phases.

4. Conclusions

Several new cinnamoyl-based photosensitive reactive mesogens with different length of the flexible terminal chain placed on the opposite side from the polymerisable double bond have been designed and synthesised. Materials have a reactive vinyl group that also allows to

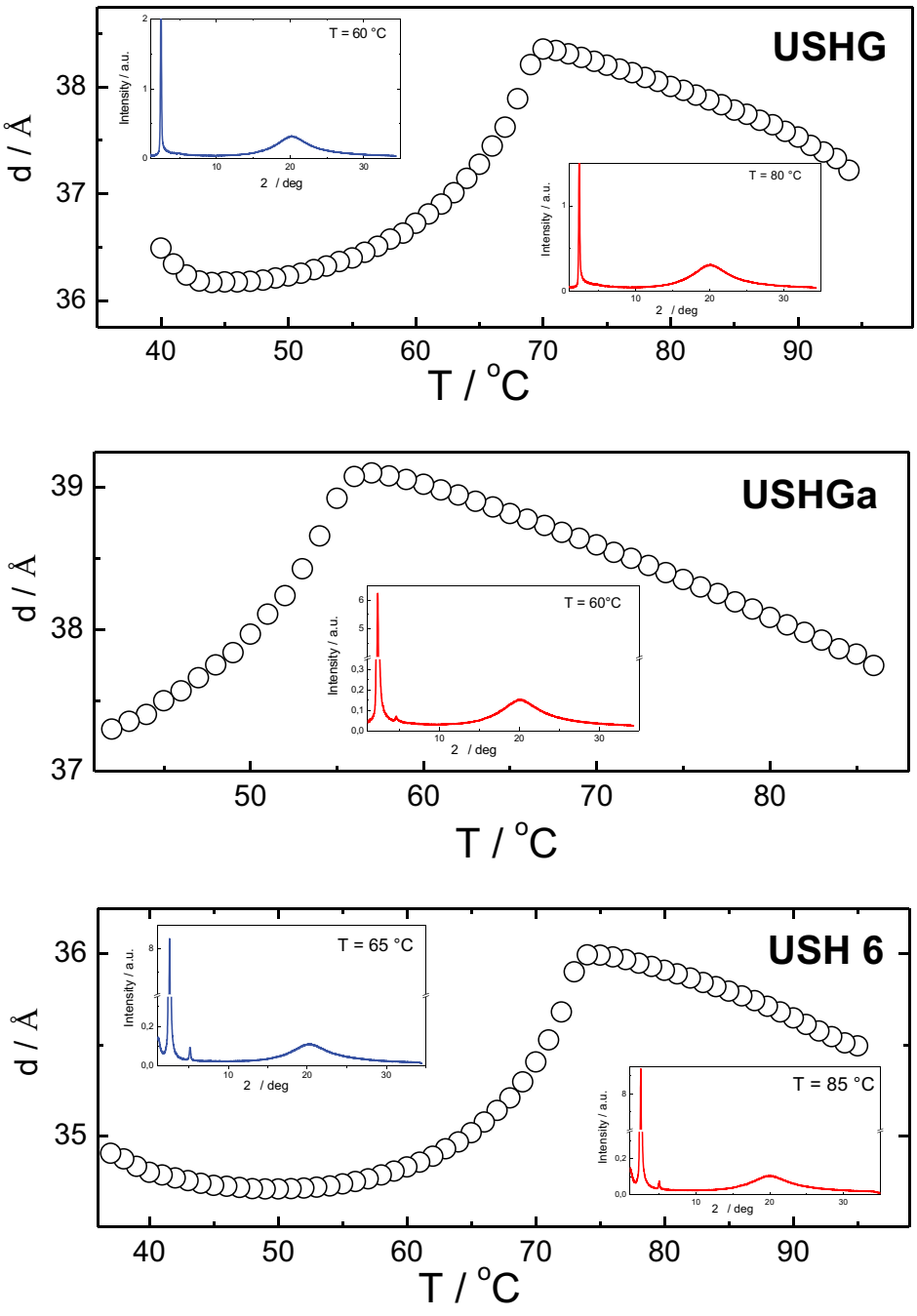

Figure 10. (Colour online) Temperature dependence of the smectic layer spacing, d, determined by the SAXS for **USHG, USHGa** and **USH 6** materials. The insets show the WAXS results of the X-ray intensity of the scattered signal versus the scattered angles at selected temperatures as indicated.

graft them on polysiloxane backbone as functional pendants of phototunable macromolecular materials [81,82].

The designed reactive mesogen with the branched alkyl chain (**USHM**) does not exhibit the LC behaviour. The other two mesogens form the nematic, the orthogonal smectic A and the tilted smectic C phases over a reasonably broad temperature range. The results of small and wide-angle X-ray scattering fully confirm the smectic phase identification based on microscopic observations.

The kinetics of the phase transition temperatures has been checked for the selected reactive mesogen. The phase transition temperatures exhibit considerable dependence on the rate of the DSC heating/cooling scans. On cooling the phase transition temperatures are slightly decreasing with the cooling rate; while

during heating, the phase transition temperatures are increasing with the higher rate.

Photoisomerisation without any other degradative processes has been the sole photoreaction confirmed in the solution phase of the designed reactive mesogens containing the cinnamoyl photosensitive fragment with C=C double bond. The results of HPLC study reveal that after UV irradiation, the ratio of the rod-like *E*-isomer and bent-shaped *Z*-isomer strongly depends on the concentration of the reactive mesogen in the original solution. Newly designed functional cinnamoyl-based photosensitive reactive mesogens can be further used for design of smart and functional self-assembling macromolecular siloxane-based materials [36], like side-chain polymers [40,83–85] and liquid single crystal elastomers [86–90] exhibiting self-assembling behaviour which can be tuned by photocycloaddition of cinnamate units. Due to the stability of the cinnamate photoproduct and the irreversible reaction, such materials can also be utilised for optical data storage and various photonic devices [91–93].

Acknowledgments

Authors greatly acknowledge the financial support from: Czech Science Foundation [Project No. CSF 19-03564S], Ministry of Education, Youth and Sports of the Czech Republic [Project No. LTC19051] and Operational Programme Research, Development and Education financed by European Structural and Investment Funds and the Czech Ministry of Education, Youth and Sports [Project No. SOLID21 - CZ.02.1.01/0.0/0.0/16_019/0000760]. Authors (N.S. and A.B.) are grateful to support of fellowship No.: 3.029 "Studium fázových přechodů nových kapalně krystalických materiálů" under "Open science 2018" programme of the Czech Academy of Sciences.

Disclosure statement

No potential conflict of interest was reported by the author(s).

Funding

This work was supported by the Czech Science Foundation [19-03564S]; Ministry of Education, Youth and Sports of the Czech Republic [LTC19051]; Operational Programme Research, Development and Education financed by European Structural and Investment Funds and the Czech Ministry of Education, Youth and Sports [SOLID21 - CZ.02.1.01/0.0/0.0/16_019/0000760]; 'Open science 2018' programme of the Czech Academy of Sciences [3.029].

ORCID

Alexej Bubnov http://orcid.org/0000-0002-6337-2210

Damian Pociecha http://orcid.org/0000-0001-7734-3181

References

[1] Lagerwall JPF, Scalia G. A new era for liquid crystal research: applications of liquid crystals in soft matter nano-, bio- and microtechnology. Curr Appl Phys. 2012;12:1387–1412.

[2] Nakayama M, Kajiyama S, Kumamoto A, et al. Stimuli-responsive hydroxyapatite liquid crystal with macroscopically controllable ordering and magneto-optical functions. Nat Commun. 2018;9:568.

[3] Herman J, Dmochowska E, Czerwiński M. Synthesis of new chiral mono- and diacrylates for ferro- and antiferroelectric liquid crystals. J Mol Liq. 2018;271:353–360.

[4] van Haaren J. Liquid crystals tilted by light. Nature. 1996;381:190–191.

[5] Akita T, Sugiyama Y, Yamazaki T, et al. Photomagnetic effects in metal-free liquid crystals. Commun Chem. 2019;2:64.

[6] Kobayashi T, Kitamoto Y, Hirai Y, et al. Light-regulated crystal growth of π-conjugated luminophores in an azobenzene matrix. Commun Chem. 2018;1:58.

[7] Zhou P, Li Y, Li X, et al. Holographic display and storage based on photo-responsive liquid crystals. Liq Cryst Rev. 2016;4:83–100.

[8] Kurp K, Tykarska M, Salamon P, et al. Design of functional multicomponent liquid crystalline mixtures with nano-scale pitch fulfilling deformed helix ferroelectric mode demands. J Mol Liq. 2019;290:111329.

[9] Bubnov A, Vacek C, Czerwiński M, et al. Design of polar self-assembling lactic acid derivatives with the keto group possessing sub-micrometre helical pitch. Beilstein J Nanotechnol. 2018;9:333–341.

[10] Kurp K, Czerwiński M, Tykarska M, et al. Design of advanced multicomponent ferroelectric liquid crystalline mixtures with sub-micrometer helical pitch. Liq Cryst. 2017;44:748–756.

[11] Czerwiński M, Urbańska M, Bennis N, et al. Influence of the type of phase sequence and polymer-stabilization on the physicochemical and electro-optical properties of novel high-tilt antiferroelectric liquid crystalline materials. J Mol Liq. 2019;288:111057.

[12] Abbott NL, Kim Y, Noh J, et al. Soft matter from liquid crystals. Soft Matter. 2019;15:6913–6929.

[13] Milewska K, Drzewiński W, Czerwiński M, et al. Highly tilted liquid crystalline materials possessing a direct phase transition from antiferroelectric to isotropic phase. Mater Chem Phys. 2016;171:33–38.

[14] Milewska K, Drzewiński W, Czerwiński M, et al. Design, synthesis and mesomorphic properties of chiral benzoates and fluorobenzoates with direct SmCA*-Iso phase transition. Liq Cryst. 2015;42:1601–1611.

[15] Żurowska M, Czerwiński M. The new high tilt mixtures with antiferroelectric phase at a broad temperature range and a long helical pitch. Liq Cryst. 2017;44:1044–1049.

[16] Czerwiński M, Tykarska M, Dąbrowski R, et al. The influence of structure and concentration of cyanoterminated and terphenyl dopants on helical pitch and

helical twist sense in orthoconic antiferroelectric mixtures. Liq Cryst. 2012;39:1498–1502.
[17] Kato T, Mizoshita N, Kishimoto K. Functional liquid-crystalline assemblies: self-organized soft materials. Angew Chem. 2006;45:38–68.
[18] Kárný M, Guy TV, Kracík J, et al. Fully probabilistic knowledge expression and incorporation. Stat Interface. 2014;7:503–515.
[19] Kárný M, Andrysek J, Bodini A, et al. How to exploit external model of data for parameter estimation? Int J Adapt Control Signal Process. 2006;20:41–50.
[20] Kárný M, Guy TV. On support of imperfect Bayesian participants. Intell Syst Ref Libr. 2012;28:29–56.
[21] Shibaev V, Bobrovsky A, Boiko N. Photoactive liquid crystalline polymer systems with light-controllable structure and optical properties. Prog Polym Sci. 2003;28:729–836.
[22] Cigl M, Bubnov A, Kašpar M, et al. Photosensitive chiral self-assembling materials: significant effects of small lateral substituents. J Mater Chem C. 2016;4:5326–5333.
[23] Poryvai A, Bubnov A, Pociecha D, et al. The effect of terminal n-carboxylate chain length on self-assembling and photosensitive properties of lactic acid derivatives. J Mol Liq. 2019;275:829–838.
[24] Klajn R. Spiropyran-based dynamic materials. Chem Soc Rev. 2014;43:148–184.
[25] Bobrovsky A, Shibaev V, Hamplová V, et al. Photoinduced phase transitions and helix untwisting in the SmC* phase of a novel cinnamoyl-based liquid crystal. Liq Cryst. 2009;36:989–997.
[26] Kurihara S, Nonaka T. Intra-and intermolecular photodimerization of mesogenic triphenylene derivative having cinnamate groups: effects of orientation and mobility of the mesogenic molecules on the photoreaction behaviour. Mol Cryst Liq Cryst Sci Technol Sect A Mol Cryst Liq Cryst. 1994;238:39–45.
[27] Oriol L, Piñol M, Serrano JL, et al. Synthesis, characterization and photoreactivity of liquid crystalline cinnamates. J Photochem Photobiol A. 2003;155:37–45.
[28] Lin C-H. Synthesis and liquid crystalline behavior of photoreactive side chain liquid crystalline polyoxetanes containing cinnamoyl biphenyl mesogen. Asian J Chem. 2015;27:1495–1500.
[29] Allen VT, Whitten DG. The photophysics and photochemistry of alpha.omega.-diphenylpolyene singlet states. Chem Rev. 1989;89:1691–1702.
[30] Bubnov A, Kašpar M, Hamplová V, et al. New liquid crystals with dichlorostilbene unit showing monotropic SmC* phase. Ferroelectrics. 2002;276:15–24.
[31] Hamplová V, Kašpar M, Pakhomov SA, et al. New series of ferroelectric liquid crystals incorporating stilbene unit in the core. Mol Cryst Liq Cryst Sci Technol Sect A Mol Cryst Liq Cryst. 1999;332:181–188.
[32] Moylan CR. Molecular hyperpolarizabilities of coumarin dyes. J Phys Chem. 1994;98:13513–13516.
[33] Schadt M, Sciberle H, Schuster A. Optical patterning of multi-domain liquid-crystal displays with wide viewing angles. Nature. 1996;381:212–215.
[34] Merlo AA, Tavares A, Khan S, et al. Liquid-crystalline coumarin derivatives: contribution to the tailoring of metal-free sensitizers for solar cells. Liq Cryst. 2018;45:310–322.
[35] Tóth-Katona T, Jánossy I. Photoalignment at the nematic liquid crystal-polymer interface: experimental evidence of three-dimensional reorientation. J Mol Liq. 2019;285:323–329.
[36] Shibaev VP, Bobrovsky A. Liquid crystalline polymers: development trends and photocontrollable materials. Russ Chem Rev. 2017;86:1024–1072.
[37] Bobrovsky A, Shibaev V, Hamplová V, et al. Gel formation and photoactive properties of azobenzene-containing polymer in liquid crystal mixture. Colloid Polym Sci. 2010;288:1375–1384.
[38] Bobrovsky A, Shibaev V, Hamplová V, et al. Photochromic and fluorescent LC gels based on a bent-shaped azobenzene-containing gelator. RSC Adv. 2015;5:56891–56895.
[39] Torres-Rocha OL, Larios-López L, Rodríguez-González RJ, et al. Synthesis and phase transitions of monomers carrying a biphenyleneazobenzene or an azotolane group. Precursors of photo-responsive liquid crystal polymers. J Mol Liq. 2017;225:251–259.
[40] Toth-Katona T, Cigl M, Fodor-Csorba K, et al. Functional photochromic liquid crystalline methylhydrosiloxane-based side-chain polymers. Macromol Chem Phys. 2014;215:742–752.
[41] Bobrovsky A, Shibaev V, Bubnov A, et al. Effect of molecular structure and thermal treatment on photo-optical properties of photochromic azobenzene-containing polymer films. Macromol Chem Phys. 2011;212:342–352.
[42] Kašpar M, Bubnov A, Hamplová V, et al. New ferroelectric liquid crystals with an AZO group in the molecular core. Liq Cryst. 2004;31:821–830.
[43] Novotná V, Hamplová V, Bubnov A, et al. First photoresponsive liquid crystalline materials with small layer shrinkage at the transition to the ferroelectric phase. J Mater Chem. 2009;19:3992–3997.
[44] Bobrovsky A, Shibaev V, Bubnov A, et al. Effect of molecular structure on chiro-optical and photooptical properties of smart liquid crystalline polyacrylates. Macromolecules. 2013;46:4276–4284.
[45] Bubnov A, Iwan A, Cigl M, et al. Photosensitive self-assembling materials as functional dopants for organic photovoltaic cells. RSC Adv. 2016;6:11577–11590.
[46] Bobrovsky A, Mochalov K, Solovyeva D, et al. Laser-induced “craters” and “hills” formation in the azobenzene-containing polymethacrylates films. Soft Matter. 2020. DOI:10.1039/D0SM00601G
[47] Chigrinov VG, Kozenkov VM, Kwok H-S. Photoalignment of liquid crystalline materials: physics and applications. John Wiley & Sons, Ltd., Chichester, England; 2008. ISBN:9780470065396. DOI:10.1002/9780470751800
[48] Hvilsted S, Sánchez C, Alcalá R. The volume holographic optical storage potential in azobenzene containing polymers. J Mater Chem. 2009;19:6641–6648.
[49] Aya S, Salamon P, Paterson DA, et al. Fast-and-giant photorheological effect in a liquid crystal dimer. Adv Mater Interfaces. 2019;6:1802032.

[50] Eremin A, Nadasi H, Hirankittiwong P, et al. Azodendrimers as a photoactive interface for liquid crystals. Liq Cryst. 2018;45:2121–2131.
[51] Palermo G, Guglielmelli A, Pezzi L, et al. A command layer for anisotropic plasmonic photo-thermal effects in liquid crystal. Liq Cryst. 2018;45:2214–2220.
[52] Jung H, Yun JH, Jeon I, et al. Acetylene-containing highly birefringent rodtype reactive liquid crystals based on 2-methylhydroquinone. Liq Cryst. 2018;45:279–291.
[53] Dong X-M, Guo J-B, Wei J. Photoreaction behaviors of two liquid crystalline cinnamoyl compounds with different phase in solution and mesomorphic states. Chinese J Chem Phys. 2010;23:719–725.
[54] Selvarasu C, Kannan P. Synthesis, characterization of azobenzene and cinnamate ester based calamitic liquid crystalline compounds and their photoresponsive properties. J Mol Struct. 2015;1092:176–186.
[55] Vojtylová T, Kašpar M, Hamplová V, et al. Chiral HPLC for a study of the optical purity of new liquid crystalline materials derived from lactic acid. Phase Transit. 2014;87:758–769.
[56] Hamplová V, Sverenyák H, Kašpar M, et al. New series of ferroelectric substances with double bond in core exhibiting helix twist inversion. Proc SPIE 3319 Liq Cryst. 1998. DOI:10.1117/12.301260
[57] Vajda A, Kašpar M, Hamplová V, et al. Phase diagrams and physical properties of binary ferroelectric mixtures based on a series of chiral α-cyanocinnamate derivatives. Liq Cryst. 2002;29:1347–1354.
[58] Hirose T, Xu Z, Kikuchi Y, et al. Polymeric fibers and microporous films by photo-crosslinking of triphenylene-derived liquid crystals. J Polym Sci Part A. 2019;57:605–612.
[59] Kohout M, Tuma J, Svoboda J, et al. 3-Hydroxycinnamic acid - a new central core for the design of bent-shaped liquid crystals. J Mater Chem C. 2013;1(32):4962–4969.
[60] Keith C, Lehmann A, Baumeister U, et al. Nematic phases of bent-core mesogens. Soft Matter. 2010;6:1704–1721.
[61] Weissflog W, Dunemann U, Findeisen-Tandel S, et al. At the boundary to banana-shaped liquid crystals: polar properties of phases formed by new asymmetric achiral four-ring bent-core mesogens. Soft Matter. 2009;5:1840–1847.
[62] Okano K, Tsutsumi O, Shishido A, et al. Azotolane liquid-crystalline polymers: huge change in birefringence by photoinduced alignment change. J Am Chem Soc. 2006;128:15368–15369.
[63] Kim J, Jung YJ, Ka J-W, et al. Mesomorphic phase transition behaviour of photopolymerisable liquid crystalline triphenylene ether compounds. Liq Cryst. 2009;36:1451–1457.
[64] Nichinori N. Design of polyimides for liquid crystal alignment films. ?Polym Adv Technol. 2000;11:404–412.
[65] He R, Wen P, Kang S-W, et al. Polyimide-free homogeneous photoalignment induced by polymerisableliquid crystal containing cinnamate moiety. Liq Cryst. 2018;45:1342–1352.
[66] Kim MW, Rastegar A, Drevensek-Olenik I, et al. Alignment of nematic liquid crystals on an electrically poled photopolymer film. J Appl Phys. 2001;90:3332–3337.
[67] Hwang J-Y, Seo D-S, Kwon O, et al. Effects of the cinnamoyl group on liquid crystal aligning capabilities on PCEMA surfaces. Liq Cryst. 2001;28:333–337.
[68] Tomita H, Kudo K, Ichimura K. Command surfaces 15 [1]. Photoregulation of liquid crystal alignment by cinnamoyl residues on a silica surface. Liq Cryst. 1996;20:171–176.
[69] Zhang L, Sun X, Liu Y, et al. Photoalignment of liquid crystals by a covalently attached self-assembled ultrathin film. Liq Cryst. 2012;39:983–991.
[70] Zhanga M, Bua X, Liua T, et al. Adjustable 2-cyano-3,4-difluoro-1H-pyrrole-based luminescent liquid crystals: synthesis, properties and substituent effect. J Mol Liq. 2018;264:425–430.
[71] Fonseca AC, Lima MS, Sousa AF, et al. Cinnamic acid derivatives as promising building blocks for advanced polymers: synthesis, properties and applications. Polym Chem. 2019;10:1696–1723.
[72] Shibaev VP. Liquid-crystalline polymer systems: from the past to the present. Polym Sci Ser A. 2014;56:727–762.
[73] Bobrovsky A, Shibaev V, Cigl M, et al. The effect of spacer and alkyl tail lengths on the photoorientation processes in amorphousized films of azobenzene-containing liquid crystalline polymethacrylates. Liq Cryst. 2020;47:377–383.
[74] Petrova I, Gaj A, Pochiecha D, et al. Design and self-assembling behaviour of comb-like stereoregular cyclolinear methylsiloxane copolymers with chiral lactate groups. Liq Cryst. 2019;46:25–36.
[75] Sulyanov SN, Dorovatovskii PV, Bobrovsky A, et al. Mesomorphic and structural properties of liquid crystalline side-chain polymethacrylates: from smectic C* to columnar phases. Liq Cryst. 2019;46:825–834.
[76] Bubnov A, Cigl M, Machado A, et al. Design of calamitic self-assembling reactive mesogenic units: mesomorphic behaviour and rheological characterisation. Liq Cryst. 2018;45:561–573.
[77] Kaur G, Johnston P, Saito K. Photo-reversible dimerisation reactions and their applications in polymeric systems. Polym Chem. 2014;5:2171–2186.
[78] Tunc D, Le Coz C, Alexandre M, et al. Photoresponsive nanogels based on photocontrollable cross-links. Macromolecules. 2014;47:8247–8254.
[79] Desvergne J-P, Bouas-Laurent H. Cycloaddition reactions involving 4n electrons: (2+2) cycloaddition; molecules with multiple bonds incorporated in or linked to aromatic systems. In: Dürr H, Bouas-Laurent H, editors. Photochromism molecules and systems. Revised ED. Amsterdam: Elsevier B.V.; 2003. p. 545. DOI:10.1002/chin.200345239
[80] Deptuch A, Jaworska-Gołąb T, Marzec M, et al. Cold crystallization from chiral smectic phase. Phase Transit. 2019;92:126–134.
[81] Hohl DK, Weder C. (De)bonding on demand with optically switchable adhesives. Adv Opt Mater. 2019. DOI:10.1002/adom.201900230

[82] Taura D, Min H, Katan C, et al. Synthesis of a double-stranded spiroborate helicate bearing stilbene units and its photoresponsive behaviour. New J Chem. 2015;39:3259–3269.
[83] Bubnov A, Kašpar M, Hamplová V, et al. New polar liquid crystalline monomers with two and three lactate groups for preparation of side chain polysiloxanes. Liq Cryst. 2006;33:559–566.
[84] Bubnov A, Novotná V, Kašpar M, et al. A liquid-crystalline siloxane based co-polymer with asymmetric bent side chains. Macromol Chem Phys. 2011;212:191–197.
[85] Bubnov A, Domenici V, Hamplová V, et al. First liquid single crystal elastomer containing lactic acid derivative as chiral co-monomer: synthesis and properties. Polymer. 2011;52:4490–4497.
[86] Domenici V, Milavec J, Zupančič B, et al. Brief overview on 2H NMR studies of polysiloxane-based side-chain nematic elastomers. Magn Reson Chem. 2014;52:649–655.
[87] Domenici V, Milavec J, Bubnov A, et al. Effect of co-monomers' relative concentration on self-assembling behaviour of side-chain liquid crystalline elastomers. RSC Adv. 2014;4:44056–44064.
[88] Milavec J, Domenici V, Zupancic B, et al. Deuteron NMR resolved mesogen vs. crosslinker molecular order and reorientational exchange in liquid single crystal elastomers. Phys Chem Chem Phys. 2016;18:4071–4077.
[89] Rešetič A, Milavec J, Domenici V, et al. Stress-strain and thermomechanical characterization of Nematic to Smectic A transition in a strongly-crosslinked bimesogenic liquid crystal elastomer. Polymer. 2018;158:96–102.
[90] Milavec J, Resetic A, Bubnov A, et al. Dynamic investigations of liquid crystalline elastomers and their constituents by 2H NMR spectroscopy. Liq Cryst. 2018;45:2158–2173.
[91] Hughes T, Simon GP, Saito K. Chemistries and capabilities of photo-formable and photoreversible cross-linked polymer networks. Mater Horizons. 2019;6:1762–1773.
[92] Felix-Serrano I, Trejo-Carbajal N, Rodríguez-González RJ, et al. Synthesis and liquid-crystalline properties of methacrylate monomers carrying a p-terphenyl laterally substituted with one or two cyano groups. J Mol Liq. 2017;241:347–354.
[93] Schelkle KM, Bender M, Beck S, et al. Photo-cross-linkable polymeric optoelectronics based on the [2 + 2] cycloaddition reaction of cinnamic acid. Macromolecules. 2016;49(5):1518–1522.